Beam dynamics in disordered $\mathcal{PT}$-symmetric optical lattices based on eigenstate analyses

Xiankun Yao[1] and Xueming Liu[1,2,3,*]

[1]*State Key Laboratory of Transient Optics and Photonics, Xi'an Institute of Optics and Precision Mechanics, Chinese Academy of Sciences, Xi'an 710119, China*

[2]*State Key Laboratory of Modern Optical Instrumentation, Department of Optical Engineering, Zhejiang University, Hangzhou 310027, China*

[3]*School of Physics and Electronic Science, Hunan University of Science and Technology, Xiangtan 411201, People's Republic of China*

(Received 4 December 2016; published 7 March 2017)

Wave functions will experience a localization process when evolving in disordered lattices. Here, we have demonstrated the effects of disordered $\mathcal{PT}$-symmetric potentials on wave-function characteristics in optics based on eigenstate analyses. In weak-disorder cases, by using the tight-binding approximation method, a conclusion is obtained that the increasing of the imaginary part of potential can enhance the diffraction, while the increasing disorder will block the diffraction and lead to localization. In the general case, band theory is used for band-structure analysis of three bands. We find that the disorder has a smaller effect on the higher-order band, which is proved by the beam evolutions. Our work may be instructive for realizing beam path control by manipulating the strengths of disorder and gain and/or loss of lattice.

DOI: 10.1103/PhysRevA.95.033804

I. INTRODUCTION

Anderson localization is the absence of diffusion of waves due to multiple scattering in a disordered medium [1–3]. The phenomenon of Anderson localization is general in physics, ranging from solid-state physics [4], acoustics [5], and matter wave physics [6,7] to optics [3,8]. In optical fields, it has been studied in severely deformed lattices [9], quasiperiodic lattices [10–12], disordered plasmonic arrays [13], and fibers [14–16]. Among them, the optical lattice is an ideal platform to explore light localization for allowing experimental implementation of controllable disorder [10–12]. Unlike the Bloch modes in a periodic lattice which are extended states, the eigenstates in a disordered lattice are localized. And the localized eigenstates have a unique property: modes near the band edges are tightly localized, whereas those near the band center are typically broader [17]. Lahini *et al.* have experimentally observed the transition from a ballistic wave-packet expansion to an exponential localization for single-site excitation [10].

Compared to conservative systems, a non-Hermitian system can produce much more interesting results for disorder-induced localization. Recent experiments observed diffusive transport, even though the non-Hermiticity lattice is periodic [18]. In pioneering papers, the delocalization transition and the existence of a mobility edge were demonstrated in non-Hermitian disordered lattices [19–22]. Such results suggest that not all the eigenstates are localized in a non-Hermitian system. Recently, robustly unidirectional light transport was realized in disordered non-Hermitian photonic lattices via a non-Hermitian delocalization transition [23].

The non-Hermitian Hamiltonians can have real eigenvalue spectra as long as they obey $\mathcal{PT}$ symmetry [24]. A necessary condition for a Hamiltonian to be $\mathcal{PT}$ symmetric is the potential function satisfying $V(\boldsymbol{x}) = V^*(-\boldsymbol{x})$. In particular, the spectra of a $\mathcal{PT}$-symmetric system possess a phase transition point below which the spectra are real and the $\mathcal{PT}$ symmetry is unbroken, and above which the spectra become partially or completely complex and the $\mathcal{PT}$ symmetry is broken [25]. Wave propagation in $\mathcal{PT}$-symmetric lattices can show a wide variety of interesting effects, such as double refraction, power oscillations, and nonreciprocity [26,27]. In a special non-Hermitian system, what would happen if disorder is introduced in a $\mathcal{PT}$-symmetric lattice? In a disordered two-dimensional lattice, the presence of $\mathcal{PT}$-symmetric potentials enhances the light localization [28]. However, Bendix *et al.* found that for a sufficiently long chain with $\mathcal{PT}$-symmetric impurities, the exact $\mathcal{PT}$-symmetric phase is retained only for an exponentially small parameter region [29]. In binary diagonal-disorder arrays, the presence of $\mathcal{PT}$ symmetry tends to inhibit the transport of localization excitations [30]. However, in the off-diagonal disordered lattice, the light localization is suppressed and restored, mediated by $\mathcal{PT}$ symmetry breaking [31]. A similar conclusion was drawn for a quasiperiodic optical lattice [32].

In this paper, we theoretically demonstrate the beam dynamics in disordered $\mathcal{PT}$-symmetry lattices. In weak-disorder cases, the coupling equation with conjugated two coupling coefficients is obtained by using the tight-binding approximation method. Through the analyses of the coupling coefficients, eigenstates, mobility edges, and beam evolutions, we can conclude that the increase of the imaginary part of the potential can enhance diffraction, while the increasing disorder will block diffraction and lead to beam localization. In general cases, the eigenstates and propagation constants for the multiband model are analyzed by using band theory. Eigenstates of the three bands have different degrees of localization where the higher band is relatively more weakly localized. Finally, that the disorder has a smaller influence on the higher-order band is proved by the beam evolutions.

II. PHYSICAL MODEL

We consider the normalized equation of diffraction with complex potential modulated by the refractive index and the

*Corresponding author: liuxueming72@yahoo.com

gains and/or losses in transverse direction. The model is governed by the Schrödinger equation [26,33,34]:

$$i\frac{\partial\psi}{\partial\xi}+\frac{1}{2}\frac{\partial^2\psi}{\partial\eta^2}+V(\eta)\psi=0, \tag{1}$$

where ξ, η are the transverse and longitudinal coordinates, respectively. The complex valued function $\psi(\xi,\eta)$ describes the electric field envelope along a propagation distance ξ. $V(\eta)=V^*(-\eta)=\sum_m(1+\delta V_m)V_0(\eta-mD)$ is an amplitude-disorder potential describing the refractive index and the gain and/or loss profile of the optical lattice, D is the regular lattice period, δV_m is the potential fluctuation depth of the mth guide (uniformly distributed in $[-W/2, W/2]$), and W determines the strength of disorder. To ensure $\mathcal{PT}$ symmetry, the complex potential of a single channel satisfies the condition $V_0(\eta)=V_0{}^*(-\eta)$ and the disorder fluctuations δV_m are set to be correlated as $\delta V_m=\delta V_{-m}$.

In this paper, we consider the optical lattice with $\mathcal{PT}$-symmetric potential of $V_0(\eta)=V_r\exp(-\eta^6/a^6)+iV_i\eta\exp(-\eta^6/a^6)$, where a is the waveguide width, and the parameters V_r and V_i are the modulation depth of refractive index and the amplitude of loss and/or gain, respectively. The system exhibits linear gain in domains with $\mathrm{Im}\{V(\eta)\}>0$ and one-photon absorption in domains with $\mathrm{Im}\{V(\eta)\}<0$. The similar potential functions have been investigated in Refs. [31,35,36] for different points. To facilitate the following study, we set $V_i=8, a=0.5$, and $D=2$; the corresponding values in realities are given in [31]. The symmetry-breaking threshold is $V_i{}^{th}\approx 18.5$ for the single site and $V_i{}^{th}\approx 16.9$ for the regular array. In the following we will analyze $\mathcal{PT}$-symmetric arrays of the weak disorders ($W\ll 1$) and general cases of disorders, separately. All the analyses are based on the so-called "unbroken $\mathcal{PT}$-symmetric phase" with only real propagating constants, because exponential growth is unavoidably excited when the $\mathcal{PT}$ symmetry is broken.

III. THEORY FOR WEAK DISORDERS

We use the tight-binding approximation method to illustrate the role of $\mathcal{PT}$-symmetric potential in the localization. The basic idea of this method is that the disordered lattice is considered as a composition of many single-site waveguides and only the interactions of adjacent-site light modes are taken into account. Consider the scattering matrix of the single-site Schrödinger operator $\hat{L}_m=(1/2)d^2/d\eta^2+V_0(\eta-mD)(1+\delta V_m)$ and the eigenvalue problem $\hat{L}_m\phi_m=\beta_m\phi_m$, where we consider the highest eigenvalue β_m as the propagating constants [37] and $\phi_m(\eta)$ represent the corresponding normalized eigenstates. The eigenstates $\phi_m(\eta)$ compose the orthogonal basis (i.e., $\int\phi_m^*(\eta)\phi_n(\eta)d\eta=\delta_{mn}, m=-N,\ldots,N$, and $2N+1$ is the number of lattice sites). Like δV_m, the propagating constants β_m are uniformly distributed with mean value β_0 and variance μ^2. The static solution of Eq. (1) can be expressed as a superposition of single-site eigenstates with different weights: $\psi_\beta(\eta,\xi)=\sum_m u_m\phi_m(\eta)\exp(i\beta\xi)$, where u_m represents the mode occupancy coefficients. By substituting this expansion into Eq. (1), multiplying by $\phi_m^*(\eta)$, and integrating over η, one can obtain a set of discrete eigen equations: $\beta u_m=\beta_m u_m+C_{m,m-1}u_{m-1}+C_{m,m+1}u_{m+1}$, where $C_{m,m\pm1}=\int_{-\infty}^{+\infty}\phi_m^*(\eta)V_m(\eta)\phi_{m\pm1}(\eta)d\eta$. For a weak-disorder lattice, i.e., $W\ll 1$, the parameters $C_{m,m\pm1}$ become independent of m to a very good approximation, so the eigen equations can be expressed as

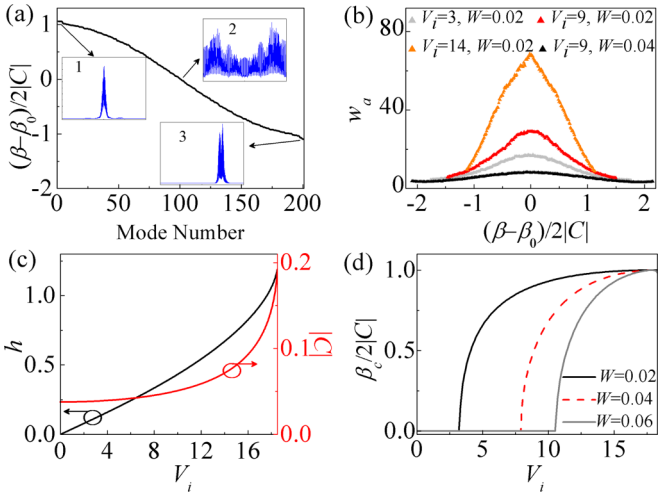

FIG. 1. Diagram of localization in weak-disorder lattices. (a) Calculated eigenstates and eigenvalues for the parameters $V_i=16$ and $W=0.02$ for one realization. Insets 1 and 3 show the localized modes formed near the edges of the band, while inset 2 denotes the extended modes near the band center. (b) Statistically averaged widths of eigenstates for various parameters of V_i and W. The phase and absolute value of coupling coefficient (c) and the mobility edges (d) vs the imaginary part of the guiding potential V_i are shown.

$$\beta u_m=\beta_m u_m+Cu_{m+1}+C^*u_{m-1}, \tag{2}$$

where $C=\int_{-\infty}^{+\infty}\phi_0^*(\eta)V_0(\eta)\phi_1(\eta)d\eta$, which can be written as $C\equiv|C|e^{ih}$. This is a typical non-Hermitian discrete equation [19,20]. Because only the fundamental mode of a single guide is considered at the start, this theoretical model is only efficient under the symmetry-breaking threshold of the optical lattice. The eigenstates and eigenvalues of the disordered lattice can be calculated by solving a set of $2N+1$ eigen equations [Eq. (2)], and $2N+1=201$ waveguides are contained in the following calculations. The eigenvalue curve is shown in Fig. 1(a) with parameters of $V_i=16$ and $W=0.02$. There is only one band calculated because only the highest eigenvalue of the single-site waveguide is considered. The eigenvalue band almost keeps the cosine shape of a perfectly ordered lattice. The eigenstates with eigenvalues near the band edges (insets 1 and 3) are exponentially localized, whereas the modes (inset 2) near the band center are typically extended; this phenomenon also arose in a Hermitian lattice [10,17]. Furthermore, the integral width of intensity $|\psi(\xi,\eta)|^2$ is calculated as $w=[\int|\psi|^2d\eta]^2/\int|\psi|^4d\eta$. For each V_i and W, we operate $Q=1000$ realizations of disordered $\mathcal{PT}$-symmetric lattices and then get the statistically average width $w_a=Q^{-1}\sum_{k=1}^{Q}w_k$. Figure 2(b) depicts the relation of average width of all the eigenstates to eigenvalues for different values of V_i and W. It is obvious that the increasing V_i and weaker disorder can broaden the mode widths. This can be explained by exploring the coupling coefficient C. In Fig. 1(c) we show the dependencies of the phase h and absolute

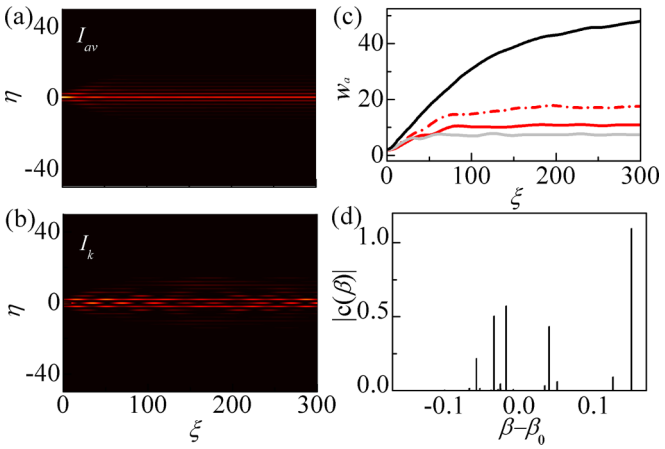

FIG. 2. Evolutions of statistically averaged intensity (a) and one illustrative realization (b) with parameters of $V_i = 9$ and $W = 0.04$. (c) Evolutions of statistically averaged beam widths with different V_i and W [solid red (solid gray) line — $V_i = 3, W = 0.02$; dash-dot red (dash-dot gray) line—$V_i = 9, W = 0.02$; black line—$V_i = 14$, $W = 0.02$; light gray line—$V_i = 9, W = 0.04$]. (d) Decomposition of input used in (a) and (b) for eigenstates in the lattice with potential distribution as in (b).

value $|C|$ of the coupling coefficient on the imaginary strength V_i of potential. When $V_i = 0$, i.e., the disordered lattice is Hermitian, the coupling coefficient C is real and $|C|$ reaches its minimum. With V_i increasing, both h and $|C|$ are enhanced, which causes diffraction to gradually dominate. In a Hermitian disordered system, the eigenstates are always localized, while the situation is changed in a non-Hermitian system when the eigenvalues fail in the region of $-\beta_c < \beta - \beta_0 < \beta_c$. The delocalization transition point β_c is called a mobility edge. Here the mobility edge can be computed as [20]

$$\beta_c \approx [4|C|^2 - \mu^2/(2|h|)]^{1/2}, \tag{3}$$

where μ^2 denotes the variance of β_m. This formula can approximately reflect the regularity of the delocalization transition. The relation of the mobility edge to V_i is shown in Fig. 1(d) for different disorder strengths of W. The imaginary part of the guiding potential is responsible for the existence of the mobility edge, and the strength of the disorder determines the value of V_i where $\beta_c > 0$ starts to occur.

In order to investigate the beam dynamistic in a disordered lattice, the statistically averaged intensity is calculated as $I_{av} = Q^{-1}\sum_{k=1}^{Q}|\psi_k|^2$. The beam propagation in the lattice can be considered as a coherent superposition of eigenstates $\psi(\xi,\eta) = \sum_\beta c(\beta)\psi_\beta(\xi,\eta)$, where the modal coefficients $c(\beta)$ can be obtained from the representation transformation $c = f/M$, where M denotes the eigenvalue matrix of Eq. (2), $f_m = \int_{-\infty}^{+\infty}\phi_m^* G(\eta)d\eta(\eta)$, and $G(\eta)$ is the input beam profile. Figure 2 depicts the beam dynamistic of the single-channel excitation, and the input is a narrow Gaussian-profile beam $G(\eta) = \exp[-(\eta/0.5)^2]$ at normal incidence. The statistically averaged intensity approaches a steady state after the initial expansion, as shown in Fig. 2(a). In each realization the intensity oscillation between several channels exists as illustrated in Fig. 2(b), which is caused by the coherent superposition of eigenstates with different propagation constants. The eigenstate coherence mentioned above determines the average widths of eigenstates and beams $\psi(\xi, \eta)$ following the same variation for various V_i and W by comparing Fig. 1(b) with Fig. 2(c). One can see that the increase of the imaginary part of the potential can enhance the diffraction by increasing the waveguide coupling, while the increasing disorder can weaken the diffraction by random scattering. Figure 2(d) shows the mode occupancy coefficients of $G(\eta)$ for the lattice with the disordered potential distribution as in Fig. 2(b). For identical $G(\eta)$, the distribution of $c(\beta)$ is specific for one realization of the lattice potential.

The tight-binding model is very effective to take the mode analysis and beam evolution for a weakly disordered lattice in a $\mathcal{PT}$-symmetric phase. However, the mentioned theory has only considered the fundamental mode of a single guide and thus there are only one-band eigenmodes calculated. In order to obtain a more generalized model, band theory will be used in the following discussion.

IV. THEORY FOR GENERAL CASES

Band theory is based on the idea that the eigenstate of a disordered lattice can be considered as the mixed state of a corresponding periodic lattice. Therefore the basic starting point in this section should be the periodic lattice. For the $\mathcal{PT}$-symmetric periodic lattice with Schrödinger operator $\hat{L}^{(0)} = 1/2d^2/d\eta^2 + \sum_m V_0(\eta - mD)$, the eigenvalue problem $\hat{L}^{(0)}\phi_{km} = \beta_{km}\phi_{km}$, where ϕ_{km} represents the normalized Floquet-Bloch (FB) modes in band m and Bloch momentum k, and β_{km} denotes the propagation constants. Here the FB modes satisfy the typical orthogonality condition of $\mathcal{PT}$ symmetry, $\int \phi^*_{-k'n}(-\eta)\phi_{km}(\eta)d\eta = d_{km}\delta_{nm}\delta_{kk'}$, where $d_{km} = \{\pm 1\}$ [26]. In the calculation with $2N+1$ waveguides contained, the Bloch wave number k is discrete for the periodic boundary condition (e.g., $k = 2\pi l/(2N+1)D$, $l = -N, \ldots, N$). For a $\mathcal{PT}$-symmetric disordered lattice, the eigenstates can be written as $\psi_\beta = \sum_{m,k} u_{km}\phi_{km}(\eta)e^{i\beta\xi}$, where u_{km} represents the mode occupancy coefficients. By substituting this expression into Eq. (1), multiplying by $\phi^*_{-km}(-\eta)$, and integrating over η, we obtain a set of discrete equations:

$$\beta u_{km} = \beta_{km}u_{km} + d_{km}\sum_{n,k'} C_{km,k'n}u_{k'n}, \tag{4}$$

where $C_{km,k'n} \approx \sum_l \delta V_l e^{ilD(k-k')}\int_{-D/2}^{D/2}\phi^*_{-km}(-\eta)V_0(\eta)\phi_{k'n}(\eta)d\eta$ represents the mode interactions, which satisfy the conjugate relation $C_{km,k'n=C^*_{k'n,-km}}$ for $\mathcal{PT}$ symmetry. Equation (4) is the eigenvalue problem, which can be solved by the numerical method. In the following calculations, only the highest three bands of the periodic lattice are considered; thus one can obtain the highest three bands of propagation constants and eigenstates of the disordered lattice by solving the eigen equation of Eq. (4). The solved propagation-constant distributions of the first three bands are shown in Fig. 3(a) for $2N+1 = 101$ waveguides with parameters of $V_i = 10$, $W = 0$ (i.e., periodic arrays, denoted by red dots), and $V_i = 10$, $W = 0.1$ (blue dots). Here the three bands are studied by band theory as a general case. From the insets one can see that the propagation constants of the higher-order band deviate more slightly from the corresponding band of

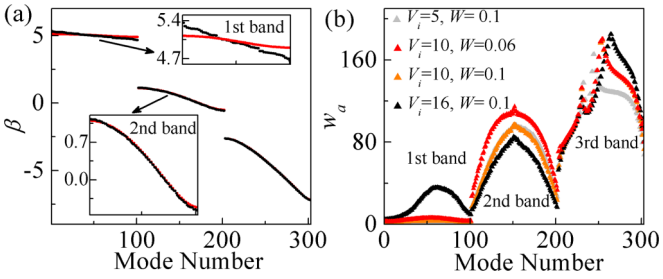

FIG. 3. Triple-band mode analysis for a disordered lattice. (a) Propagation constant distributions for parameter $V_i = 10$ [red (gray) dots—periodic arrays, black dots—disordered arrays with $W = 0.1$]. Insets are the enlarged pictures of propagation constants for the first and second bands. (b) Averaged widths of eigenstates for different combinations of V_i and W.

the periodic lattice compared to the lower-order band. And the averaged eigenstate widths of the higher-order band are bigger than the lower-order band, as shown in Fig. 3(b). For a higher-order band such as the second and third bands, the eigenstates near the band centers are much broader than the eigenstates near band edges, as the eigenstates of the first band did when discussed in the weak-disorder case. The averaged eigenstate widths of the second band are mainly dominated by the disorder strength W, while the averaged widths of the third band are mainly determined by the amplitude of the imaginary potential V_i, which seems to imply that the disorder has a smaller effect on the third band than the second band. The specific eigenstate distributions are displayed in Fig. 4 for the first three bands. One can see that the higher the order of the band, the broader the eigenstates, and the eigenstates near the band centers are much broader than the eigenstates near band edges, which coincides with the description in Fig. 3(b).

From the analysis above, it seems that the disorder has a smaller effect on the higher-order band. To confirm this, we

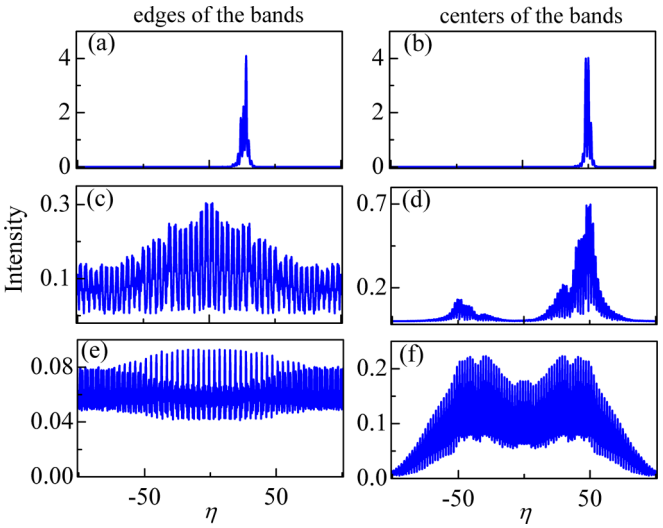

FIG. 4. One realization of the eigenstate distributions for a disordered lattice with $V_i = 10$, $W = 0.1$. The curves in (a) (b), (c) (d), and (e) (f) are the eigenstates in the first, second, and third band, respectively. (a, c, e) The centers of the corresponding bands; (b, d, f) the edges of the bands.

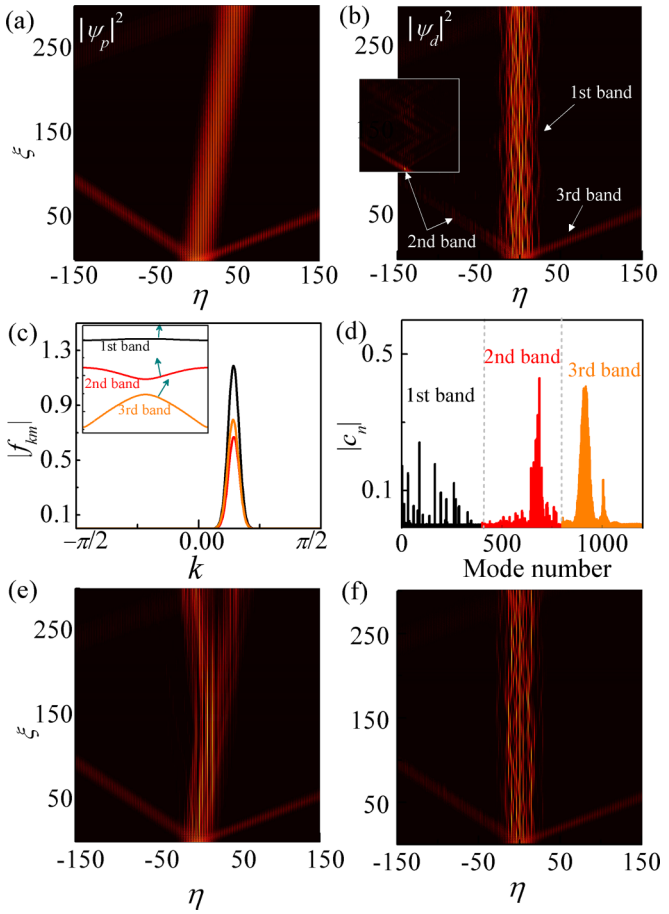

FIG. 5. The intensity evolutions of a wide tilt beam exciting the periodic (a) and disordered (b, e, f) lattices. The inset of (b) is the individual propagation of the second band on a smaller scale of color bar. (c) FB decomposition of the input in (a) for the first three bands [black line–1st, red (gray) line–2nd, orange (light gray) line–3rd), and the inset shows the corresponding band structure. (d) Disordered lattice eigenstate decomposition of the input in (b) for three bands. Here $V_i = 10$ and $2N + 1 = 401$ in all cases, and $W = 0.1, 0.01$, and 0.05 for the disordered lattices of (b), (e), and (f), respectively.

investigate the beam evolutions in the periodic and disordered $\mathcal{PT}$ -symmetric state when excited by one identical wide tilt beam of incidence, as shown in Fig. 5. The input can be approximately regarded as a Gaussian-shape beam, with beam width of 30.7 and tilt angle of 24° in homogeneous media. The intensity evolutions in Fig. 5 have three pathways due to the double-refraction process that has been studied in Ref. [26]. For an input beam profile $G(\eta)$, its beam evolutions can be expressed as

$$\psi_p(\eta,\xi) = \sum_{m,k} f_{km}\phi_{km}(\eta)e^{i\beta_{km}\xi},$$
$$\psi_d(\eta,\xi) = \sum_{n} c_n\psi_{\beta_n}(\eta)e^{i\beta_n\xi}, \quad (5)$$

in periodic and disordered lattices, respectively, where β_n is the propagation constant of the nth eigenstate of the disordered lattice, $f_{km} = \int \phi^*_{-km}(-\eta)G(\eta)d\eta$, and the coefficients c_n are the mode occupancy coefficients in periodic-lattice and

disordered-lattice representations, respectively, which can be obtained by representation transformation of f_{km} through the eigenvalue matrix of Eq. (4). Figures 5(c) and 5(d) depict the occupancy $|f_{km}|$ and $|c_n|$ (among bands), respectively, corresponding to the same input used in Figs. 5(a) and 5(b), respectively.

Keeping in mind that the beam components in the periodic lattice will propagate along the gradient $\nabla_k(\beta)$, one can then distinguish from the inset in Fig. 5(c) which pathway corresponds to which band in Fig. 5(a). The influence of disorder on beam dynamics can be illustrated by comparing to Figs. 5(b), 5(e), 5(f), and 5(a). Comparing the first-band components, i.e., the beams of the middle paths in these figures, the beam propagates in the periodic lattice at a tilt angle, while the propagation is partially deviated in the lattice with weak disorder shown in Fig. 5(e), and the beam propagates vertically and the transverse transport disappears in the lattices with relatively stronger disorder, as shown in Figs. 5(b) and 5(f). That is because the scattering from disorder brings the transverse transport of the first band to a partial or complete halt. The left propagations are the second-band components. The propagations of the second-band components in periodic and weak-disorder lattices are very smooth [Figs. 5(a), 5(e), and 5(f)], while when the disorder strength increases to $W = 0.1$, the evolution becomes weaker and weaker when traversing across the lattice, which is displayed in Fig. 5(b). The wave packets are partially obstructed by multiple reflections and the residual can traverse across the disordered lattice; the inset of Fig. 5(b) depicts the details. Different from the first two bands, the third-band components, i.e., the beams spreading toward the right, show almost no difference when comparing Figs. 5(b), 5(e), and 5(f) to Fig. 5(a). Therefore one can say that the lattice disorder has less impact on the third-band component of the wide beam. Figures 5(c) and 5(d) illustrate the eigenstate decompositions of the input beam in the representations of the periodic lattice and the disordered lattice in Fig. 5(b), respectively. The distribution of first-band decomposition is completely skewed by disorder, while the second and third bands partially retain their configurations, as seen by comparing Fig. 5(d) to Fig. 5(c).

Comparing the tight-binding approximation in Sec. III with the band theory here, they focus on different points. In Sec. III, the point is the localization characteristics of eigenstates and beam evolutions in a disordered lattice. The delocalization of eigenstates only arises in weak disorder. With the disorder strength increasing, the eigenstates near the band center are localized rapidly. The tight-binding model is very effective to the lattice in the weak-disorder region, the calculation process is relatively simple, and the mobility edges can be deduced in this theory. However, this model has considered only the fundamental mode of a single-site waveguide; thus there are only one-band eigenstates calculated [37]. In Sec. IV, the point is eigenstate distribution and beams dynamics in different bands. The band theory is a more generalized model as more bands are calculated, and the amount of computation is much larger than the tight-binding model.

V. CONCLUSIONS

In conclusion, we have demonstrated that disordered $\mathcal{PT}$-symmetry potentials can exhibit unique characteristics in optics. In weak disorder cases, the coupling equation with conjugated two coupling coefficients is obtained by using the tight-binding approximation method. The localization character is analyzed by studying the eigenstates, mobility edges, and beam evolutions by using the tight-binding approximation method. A conclusion is obtained that the increase of the imaginary part of the potential can enhance the diffraction, while the increasing disorder will block the diffraction and lead to localization. In the general case, band theory is used for band-structure analysis. We find that the disorder has a smaller effect on the higher-order band, which is proved by the beam evolutions. These results will be potentially instructive for further researchers. For fundamental interest, it reveals the nature of localization-delocalization transitions and band-structure characteristics in disordered $\mathcal{PT}$-symmetry optical lattices. For practical use, it may pave the way for realizing beam path control by manipulating the strengths of disorder and gain and/or loss. The results in this paper are very possible to be raised in other quasiperiodic physical systems, such as plasmonic waveguides, cavity polaritons, and bulk metamaterials. Moreover, in future research, it would be interesting to study the nonlinear phenomena in disordered lattices, such as soliton behavior.

ACKNOWLEDGMENTS

This work was supported by the National Natural Science Foundation of China under Grant No. 61525505 and by the Key Scientific and Technological Innovation Team Project in Shaanxi Province under Grant No. 2015KCT-06.

[1] P. W. Anderson, Phys. Rev. **109**, 1492 (1958).
[2] S. John, Phys. Rev. Lett. **53**, 2169 (1984).
[3] M. Segev, Y. Silberberg, and D. N. Christodoulides, Nat. Photon. **7**, 197 (2013).
[4] A. S. C. Rittner and J. D. Reppy, Phys. Rev. Lett. **98**, 175302 (2007).
[5] H. Hefei, A. Strybulevych, J. M. Page, S. E. Skipetrov, and B. A. van Tiggelen, Nat. Phys. **4**, 945 (2008).
[6] J. Billy, V. Josse, Z. C. Zuo, A. Bernard, B. Hambrecht, P. Lugan, C. Clement, L. Sanchez-Palencia, P. Bouyer, and A. Aspect, Nature (London) **453**, 891 (2008).
[7] S. S. Kondov, W. R. McGehee, W. Xu, and B. DeMarco, Phys. Rev. Lett. **114**, 083002 (2015).
[8] D. S. Wiersma, Nat. Photon. **7**, 188 (2013).
[9] D. S. Wiersma, P. Bartolini, A. Lagendijk, and R. Righini, Nature (London) **390**, 671 (1997).
[10] Y. Lahini, A. Avidan, F. Pozzi, M. Sorel, R. Morandotti, D. N. Christodoulides, and Y. Silberberg, Phys. Rev. Lett. **100**, 013906 (2008).
[11] T. Schwartz, G. Bartal, S. Fishman, and M. Segev, Nature (London) **446**, 52 (2007).

[12] A. S. Pikovsky and D. L. Shepelyansky, Phys. Rev. Lett. **100**, 094101 (2008).
[13] X. Shi, X. Chen, B. A. Malomed, N. C. Panoiu, and F. Ye, Phys. Rev. B **89**, 195428 (2014).
[14] T. Pertsch, U. Peschel, J. Kobelke, K. Schuster, H. Bartelt, S. Nolte, A. Tünnermann, and F. Lederer, Phys. Rev. Lett. **93**, 053901 (2004).
[15] S. Karbasi, C. R. Mirr, P. G. Yarandi, R. J. Frazier, K. W. Koch, and A. Mafi, Opt. Lett. **37**, 2304 (2007).
[16] S. Karbasi, R. J. Frazier, K. W. Koch, T. Hawkins, J. Ballato, and A. Mafi, Nature Commun. **5**, 3362 (2014).
[17] F. M. Izrailev, S. Ruffo, and L. Tessieri, J. Phys. A: Math. Gen. **31**, 5263 (1998).
[18] T. Eichelkraut, R. Heilmann, S. Weimann, S. Stu¨tzer, F. Dreisow, D. N. Christodoulides, S. Nolte, and A. Szameit, Nat. Commun. **4**, 2533 (2013).
[19] N. Hatano and D. R. Nelson, Phys. Rev. Lett. **77**, 570 (1996).
[20] P. W. Brouwer, P. G. Silvestrov, and C. W. J. Beenakker, Phys. Rev. B **56**, R4333 (1997).
[21] N. Hatano and D. R. Nelson, Phys. Rev. B **58**, 8384 (1998).
[22] A. Basiri, Y. Bromberg, A. Yamilov, H. Cao, and T. Kottos, Phys. Rev. A **90**, 043815 (2014).
[23] S. Longhi, D. Gatti, and G. Valle, Sci. Rep. **5**, 13376 (2015).
[24] C. M. Bender and S. Boettcher, Phys. Rev. Lett. **80**, 5243 (1998).
[25] A. Guo, G. J. Salamo, D. Duchesne, R. Morandotti, G. Siviloglou, and D. Christodoulides, Phys. Rev. Lett. **103**, 093902 (2009).
[26] K. G. Makris, R. El-Ganainy, D. N. Christodoulides, and Z. H. Musslimani, Phys. Rev. Lett. **100**, 103904 (2008).
[27] S. V. Suchkov, A. A. Sukhorukov, J. Huang, S. V. Dmitriev, C. Lee, and Y. S. Kivshar, Laser Photon. Rev. **10**, 177 (2016).
[28] D. M. Jović, C. Denz, and M. R. Belić, Opt. Lett. **37**, 4455 (2012).
[29] O. Bendix, R. Fleischmann, T. Kottos, and B. Shapiro, Phys. Rev. Lett. **103**, 030402 (2009).
[30] C. Mejia-Cortes and M. I. Molina, Phys. Rev. A **91**, 033815 (2015).
[31] Y. V. Kartashov, C. Hang, V. V. Konotop, V. A. Vysloukh, G. Huang, and L. Torner, Laser Photon. Rev. **10**, 100 (2016).
[32] C. Hang, Y. V. Kartashov, G. Huang, and V. V. Konotop, Opt. Lett. **40**, 2758 (2015).
[33] Y. V. Kartashov, V. A. Vysloukh, and L. Torner, Phys. Rev. Lett. **96**, 073901 (2006).
[34] K. G. Makris, Z. H. Musslimani, D. N. Christodoulides, and S. Rotter, Nat. Commun. **6**, 7257 (2015).
[35] A. Szameit, Y. V. Kartashov, P. Zeil, F. Dreisow, M. Heinrich, R. Keil, S. Nolte, A. Tünnermann, V. A. Vysloukh, and L. Torner, Opt. Lett. **35**, 1172 (2010).
[36] S. Stützer, Y. Kartashov, V. A. Vysloukh, V. V. Konotop, S. Nolte, L. Torner, and A. Szameit, Opt. Lett. **38**, 1488 (2013).
[37] G. Del Re, Theoret. Chim. Acta **1**, 188 (1963).